Indian Journal of Pure & Applied Physics
Vol. 61, March 2023, pp. 198-205
DOI: 10.56042/ijpap.v61i3.71225

Polyaniline Chromium Nitrate Composites: Influence of Chromium Nitrate on Conductivity and Thermal Stability of Polyaniline

Asha[a*], Sneh Lata Goyal[b], Rishi Pal[b], Shashi Kala Gupta[c], Rahul Sharma[d] & Rachna Dhankhar[e]

[a]Department of Basic and Applied Sciences, Bhagat Phool Singh Mahilla Vishwavidyalaya, Khanpur Kalan (Sonipat), Haryana-131 305, India

[b]Department of Physics, Guru Jambheshwar University of Science and Technology, Hisar, Haryana-125 001, India

[c]Department of Chemistry, Shri Govind Singh Gurjar Government College, Nasirabad, Ajmer, Rajasthan-305 601, India

[d]CSIR- National Physical Laboratory, New Delhi-110 012, India

[e]Department of Chemistry, Maharashi Dayanand University, Rohtak, Haryana-124 001, India

Received 8 February 2023; accepted 27 February 2023

Thermal stability and electrical conductivity are the key to the technological feasibility and sustainability of conducting polymers (CPs) and their composites in real-time applications. Notably, the impact of filler loading on above mentioned parameters of CPs needs to be examined and addressed with facile and easily accessible techniques. In the present study, Polyaniline (PANI) /chromium nitrate composites have been prepared via in situ polymerization of aniline through the chemical oxidative polymerization route. After that, the conductivity and thermal stability of PANI have been investigated at different weight percentage loadings of chromium nitrate viz 5, 10, 20, and 40 % in the composite materials. The morphological and structural analysis of the pristine and composite samples were executed with Scanning electron microscopy (SEM), Fourier transforms infrared (FTIR) spectroscopy, and X-ray diffraction (XRD) techniques. Thermal analysis of proposed composites is carried out using the thermogravimetric analysis (TGA) method to evaluate various kinetic parameters. The TGA thermogram and different calculated parameters revealed that the composites were more thermally stable than pristine PANI and that the composite having 20 wt % of chromium nitrate is thermally the most stable. The DC electrical conductivity data shows that PANI loaded with 20% chromium nitrate has the highest conductivity. This increment in conductivity and thermal stability of the composites opens the path for many applications, such as sensors and electronics.

Keywords: Polyaniline; Chromium nitrate; Structural characterization; Thermal stability; DC electric conductivity

1 Introduction

Polyaniline (PANI) has been the focus of attention of researchers for the past few decades owing to its facile synthesis and unique electrical-thermal-mechanical and optoelectronic properties. Consequently, it has been extensively studied in numerous scientific applications ranging from sensing[1,2], photo-catalysis[3,4], anti-corrosion coatings, fabrication of semiconductor devices (diodes, transistors, LED, *etc*.)[5], EMI (Electromagnetic Interference) shielding[6-9], electrochromic devices[10] and rechargeable batteries, etc. Interestingly, the properties and applications of polyaniline can be improved upto a considerable extent through controlled designing of its composite forms[1-12]. Therefore, in recent times, more efforts have been paid to synthesizing and characterizing polyaniline and its composites. For instance, WO_3/PANI composite films synthesized by the double pulse deposition method showed an increased conductivity compared to WO_3[10]. PANI becomes more thermally stable, and its structural, electrical, and optical properties improve in its composites with transition metal oxide composites like In_2O_3[11], TiO_2[3,4,12,14], ZnO[4,15] and CuO[1,13,] *etc*. The composites mentioned above have shown promising potential in various applications such as corrosion protection, sensors, and photocatalytic degradation of environmental contaminants like dyes, organic compounds, etc.[1-5,13,16,17]. Also, PANI, in its composite form with various metal oxide semiconductors like In_2O_3, TiO_2, ZnO, and Bismuth oxide, has excellent thermal, optical, and electrical properties[5,14,15,19]. Hence, it can be used in various applications, viz. sensors, EMI shielding, corrosion protection, and fabrication of semiconductor devices, *etc*.[5,7,9,19]. Chromium nitrate has potential applications in agriculture, making catalysts, corrosion inhibitors,

*Corresponding authors: (E-mail: arana5752@gmail.com)

dyeing industry, and textile printing[20,21]. Being a relatively inert material and due to its excellent aqueous phase, processability Chromium Nitrate is recognized to be a perfect filler for PANI-based composites. To the authors' knowledge, no report has been done on the synthesis and characterization of PANI/chromium nitrate composites.This paper examines the proposed PANI/ chromium nitrate composites through facile and easy-to-use characterization techniques like FTIR, XRD, SEM, TGA, etc. Moreover, an in-depth analysis has been carried out on the impact of chromium nitrate content on the PANI's electrical conductivity and thermal stability.

2 Experimental Details

2.1 Synthesis of PANI

PANI is synthesised using the chemical oxidative polymerization route. In a typical experiment, 0.2 M aniline hydrochloride (Sigma Aldrich 99.99 % purity) and oxidant 0.25 M ammonium persulphate (Sigma Aldrich 99.99% purity), aqueous solutions were mixed adequately with continuous stirring between temperature ranges (0-4) °C on an ice bath. The polymerization process was further carried out at room temperature. To ensure complete polymerization, the reaction mixture was kept overnight. The resulting PANI compound was filetered, and vacuum dried at 45 °C and named C0[14, 15].

2.2 Synthesis of PANI/Chromium Nitrate composites

PANI/Chromium nitrate composites are synthesized by mixing 5, 10, 20, and 40 weight% of 0.1M chromium nitrate in aniline hydrochloride and following the same procedure mentioned for PANI. The synthesized composites are named C1, C2, C3, and C4.

2.3 Analytical Techniques

The above-prepared samples were characterized using a Rigaku Table-Top X-Ray diffractometer for X-ray diffraction study Microtrac Semtrac Mini Scanning Electron Microscope for morphological analysis. Schimadzu IR affinity-1 8000 for FTIR study. TA SDT Q600 for Thermogravimetric analysis in a nitrogen atmosphere and Keithley 6517A Electrometer for DC conductivity measurements.

3. Results and Discussion

3.1 X-ray Diffraction (XRD) Analysis

X-ray studies have been used to analyze the structural properties of prepared samples in the pristine form of PANI and its doped form (C0-C4). Fig. 1(a) represents the pristine chromium nitrate XRD pattern, indicating that the used chromium nitrate chemical is highly crystalline. The XRD pattern of chromium nitrate consists of many highly intense peaks at 2θ angles of ~14.02°, 18.10°, 22.44°, 29.22°, 35.46°, 38.86°, 47.82°, and 67.49°. The particle size of chromium nitrate has been computed with the help of Scherrer's formula and peaks at 22.44° [15,21,22]

$$\Delta = \frac{0.91\lambda}{\beta\cos\theta} \quad ...(1)$$

The size of crystallite estimated with the help of Scherrer's formula is 33.6 nm suggesting the nanocrystalline behavior of the chromium nitrate particles. It is observed from Fig. 1(b) that every sample has a broad band situated around 25° with a sharp peak plus the two shoulders at angles 2θ ≈ 21° and 16°. The characteristic peaks of PANI shown by the XRD reflections at 16°, 25° and 21° are accredited to the (011), (200), and (020) planes of PANI[21-25]. A sharp peak on the broad hump in XRD patterns of every sample impliesthe semi-crystalline nature of the samples.

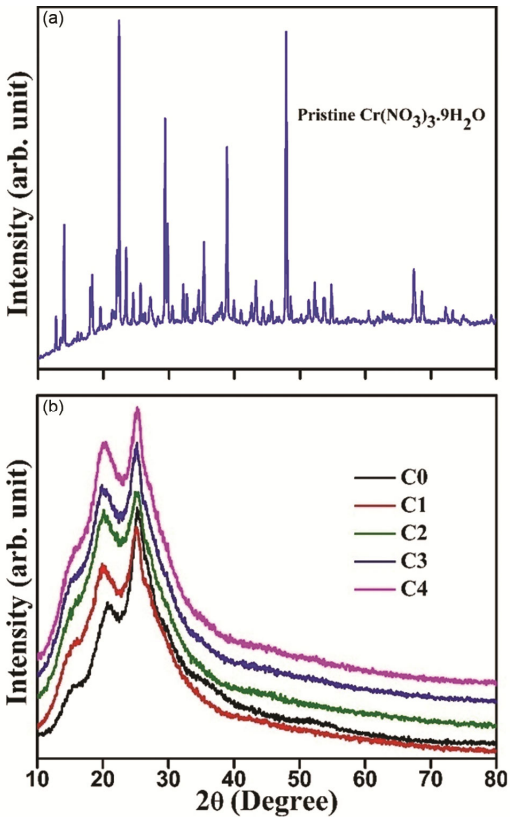

Fig. 1 — XRD pattern of (a) Chromium nitrate and (b) PANI and PANI/ chromium nitrate composites.

In these composites, the quinoid and benzenoid rings present in the vertical and horizontal directions lead to short periodicity. The reappearance of these planes in the vertical and horizontal directions occurrence of four characteristic peaks gives rise to the semi-crystalline nature of PANI and its composites. The band situated at 21° could be due to the presence of the parallel or horizontal periodicity of the benzene rings present in polymer chains, and they are related to the inter-planer spacing of the benzene rings with the adjoining chains' or'close contact inter-chain distance, while, the presence of sharp reflection at 25° could be due to the presence of polymer chains perpendicular periodicity[21-25].

Moreover, with increasing concentrations of chromium nitrate in the composites, the primary peak in XRD shifts slightly towards the right showing a decrease in crystallite size and an increase in lattice strain.

3.2 Fourier Transform Infrared (FTIR) Analysis

FTIR spectra of PANI and PANI loaded with 5%, 10%, 20%, and 40% by weight of chromium nitrate arepresented in Fig. 2 to understand the effect of loading of chromium nitrate on PANI. The FTIR spectrum of PANI displays unusual vibrations in the range of 500-1700 cm^{-1}. The main bands are at 815, 520, 1317, 1163, 1589 and 1495 cm^{-1}. The bands in the lower frequency range are 815 cm^{-1} and520 cm^{-1}. The main reason for these bands is the para-disubstituted aromatic rings and C-H out-of-plane bending vibration correspondingly[26-28]. The C-N stretching vibrations are indicated by a band near 1317 cm^{-1} [27,28]. The C-H in-plane bending vibration appears[25] at 1163 cm^{-1}. The appearance of the bands in the range of 1450-1600 cm^{-1} is because of the non-symmetric C_6 ring stretching modes[25,27].The band at 1589 cm^{-1} is attributed to the presence of the quinoid rings, while the band at a lower frequency, 1495 cm^{-1} is assigned due to benzenoid rings[25]. The peak that appeared at 2300 cm^{-1} is because of aromatic C-H stretching vibrations, whereas the band observed between 2950-3300 cm^{-1} is attributed to aromatic amines N-H stretching[25].

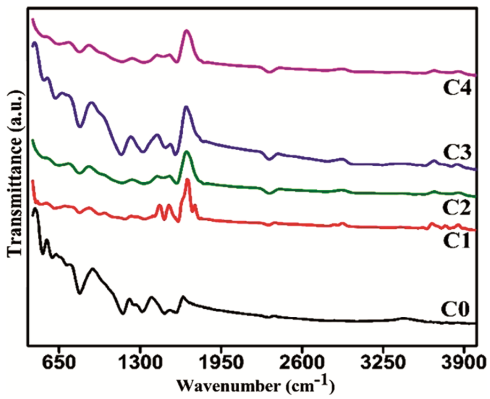

Fig. 2 — FTIR spectra of PANI and PANI/$Cr(NO_3)_3$ composites.

In the FTIR spectrum of PANI/$Cr(NO_3)_3$ composites, the nitrate group has six normal vibrations that are IR active. They are the out-of-plane bending, antisymmetric stretching, antisymmetric in-plane bending, symmetric stretching, symmetric in-plane bending, and totally symmetric stretching observed at 870, 1629, 729, 1388, 664, and 1052 cm^{-1}, correspondingly[29,30]. Due to the presence of water content, OH stretching and OH_2 scissors frequencies are observed at about 3500 cm^{-1} and 1600 cm^{-1}[27-29].

Peaks at some of these positions already exist in PANI. So, in composites, these peaks mix with the PANI peaks. But an extra peak at 1052 cm^{-1} is also visible in composites. Also, a slight shift in the positions of bands of PANI is observed in the FTIR spectra of composites. Consequently, the FTIR results confirmed the presence of chromium nitrate in PANI.

3.3 Scanning Electron Microscopy (SEM)

The scanning electron micrograph of PANI and PANI/$Cr(NO_3)_3$ is shown in Fig. 3. A perusal of the figure shows that the SEM images in the two cases differ, suggesting the formation of composite[30,31]. Bigger-sized object in the composites indicates cluster formation[30]. Consequently, the SEM results substantiate the existence of chromium nitrate in composites.

3.4 Thermogravimetric Analysis (TGA)

A TGA thermogram of PANI and PANI/$Cr(NO_3)_3$ composites in a nitrogen atmosphere is shown in Fig. 4.

The TGA analysis of PANI/$Cr(NO_3)_3$ composites specifies the four steps for weight loss.

1. Initially, the loss in weight is at about 100 °C, called the first dehydrating stage. This weight loss is due to water desorption absorbed at the polymer matrix surface[14,31].
2. The second stage of weight loss is observed at about 250 °C. This may be due to protonic acid component degradation in the sample[14,31].
3. The third and fourth stage of weight loss was observed at about 500 °C and 600 °C, showing the polymer linkage breaking resulting in the production of gases[14,15,32].

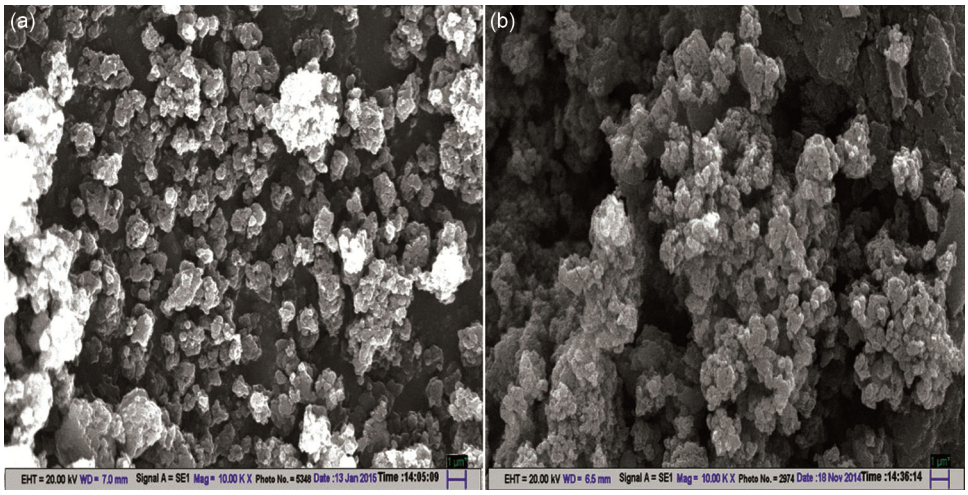

Fig. 3 — SEM of (a) PANI (b) PANI/$Cr(NO_3)_3$ composite (C2).

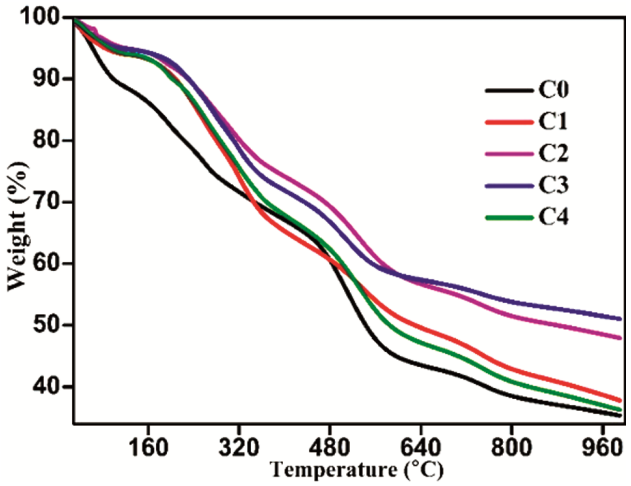

Fig. 4 — TGA thermo grams of PANI and PANI/$Cr(NO_3)_3$ composites.

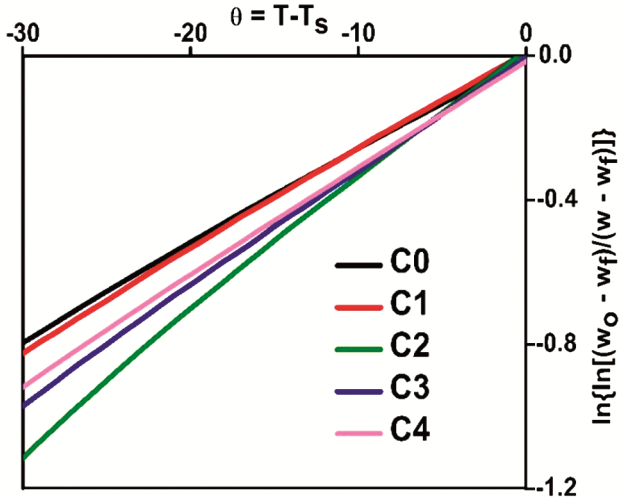

Fig. 5 — Plot of ln $[\ln\left(\frac{w_0-w_f}{w-w_f}\right)]$ *vs.* θ for PANI and PANI/$Cr(NO_3)_3$composites.

To study the thermal properties, different kinetic parameters for study have been calculated and are explained here:

Activation Energy (E_a)

The thermal activation energy E_a can be determined with the help of equation (2), given as

$$ln\,[\,ln\left(\frac{w_0-w_f}{w-w_f}\right)] = \frac{E_a\theta}{RT_s^2} \qquad \ldots(2)$$

where w is the remaining weight at T temperature, w_0 is the initial weight, E_a is the thermal activation energy, w_f is the final weight, R is gas constant, and θ = $T-T_s$ with T_s as the reference temperature corresponding to $\left(\frac{wa-w_f}{w_0-w_f}\right)$ = 1/e.

Using the above equation, thermal activation energy could be determined by the slope of the straight line fitted in between θ and ln $[\ln\left(\frac{w_0-w_f}{wn-w_f}\right)]$ as demonstrated in Fig. 5 (for Pure PANI and PANI/$Cr(NO_3)_3$ composites)[14,27].

The value of thermal activation energy obtained has been listed in Table 1. The table shows that the thermal activation energy first varies directly with the content of chromium nitrate up to 20 percent by weight and then varies inversely with varying chromium nitrate concentration. The rise in thermal activation energy implies anenhancement in the polymer's thermal stability, whereas the decrement in thermal activation energy means adecrement in thermal stability[27,33]. This increment in thermal activation energy up to C2 could be due to the packing density increase and molecular arrangements reorganization in the polymeric sample; after that, the

Table 1 — Values of different kinetic parameters for PANI and PANI/$Cr(NO_3)_3$ composites

Sample	E_a(KJ/mol)	A (10^{10}) (s^{-1})	ΔS(J/mol/K)	ΔG(KJ/mol)
C0	136.714	0.093	-187.568	286.393
C1	152.734	0.198	-173.290	293.099
C2	172.532	7.648	-102.933	254.158
C3	184.481	41.508	-70.019	262.874
C4	168.148	3.578	-117.529	261.584

Table 2 — DC Conductivity of PANI and PANI/$Cr(NO_3)_3$composites at 1V at various temperatures

Temp (K)	Conductivity (×10^{-4}) (S/cm)				
	C0	C1	C2	C3	C4
313	1.91	8.61	17.11	20.72	13.59
333	2.10	9.66	18.06	21.80	14.15
353	2.42	11.26	19.09	22.23	14.73
373	2.73	12.81	19.62	22.72	15.26
393	2.91	13.66	20.22	23.26	15.85

decrease could be because of the imperfections in the lattice.

Frequency Factor (A)

The value of the frequency factor can be determined with the help of equation (3) which is mentioned below

$$A = \frac{\beta E_a}{RT_s^2} \exp\left(\frac{E_a}{RT_s}\right) \quad \ldots(3)$$

here β is the constant heating rate, and A is the frequency factor. The values calculated for the frequency factor are mentioned in Table 2. Evidently, the value for the frequency factor from the table, like thermal activation energy, rises with the increment of chromium nitrate content up to 20 percent by weight, and then it reduces. The increment in the frequency factor implies an increment in the reaction rate, and the decrement indicates the reverse behaviour. The increment could be due to the polymeric chains scissoning, thereby increasing the reaction rate with the increase in the chromium nitrate concentration[14,34,] and the decrease could be due to the imperfections in the lattice.

Entropy of Activation (ΔS)

The value for activation entropy may be calculated by the use of equation (4) which is given as

$$\Delta S = 2.303\, R\, log\, (\frac{Ah}{kT_s}) \quad \ldots(4)$$

Where k is Boltzmann constant and h is Planck's constant, the calculated results are represented in Table 1. Analyzing the presented data in Table 1, initially, there is an enhancement in activation entropy with the increase in $Cr(NO_3)_3$ concentration and then attains maxima corresponding to the 20 percent by weight of chromium nitrate. Further, it starts reducing with a further rise in $Cr(NO_3)_3$concentration[34,35]. The entropy of activation increment with increasing concentration of $Cr(NO_3)_3$ proposes the increment in reaction rate, and its decrease shows the reverse trend. Further, the ΔS negative value specifies that the resultant complex has a more ordered structure than the reactants[14,15].

Free Energy of Change of Decomposition (ΔG)

The value for free energy change of decomposition may be calculated with the help of equation (5) given below

$$\Delta G = E_a - T_s \Delta S \quad \ldots(5)$$

The values then calculated are demonstrated in Table 1. ΔG has a positive value in the case of PANI/$Cr(NO_3)_3$ composites, showing that the degradation reaction is non-spontaneous[27,34].

3.5 DC Conductivity

Current (I) - Voltage (V) characteristics of PANI and PANI loaded with Cr $(NO_3)_3$ at different temperatures and concentrations are shown in Fig. 6(a) & (b). The Persual of the figure shows an anon-linear current increase with applied voltage. The conduction mechanism in such PANI is not the same as intrinsic semiconductors[35]. The polymer matrix's added positive and negative charges in PANI do not fill the valence and conduction band. In fact, random-polaron trapping is responsible for conduction in PANI in place of permanent dipoles

As an effect of the applied external field because of the strong coupling in phonons and electrons, the lattice distortions occur around the doped charge[14,36]. Due to these lattice distortions, there are stronger

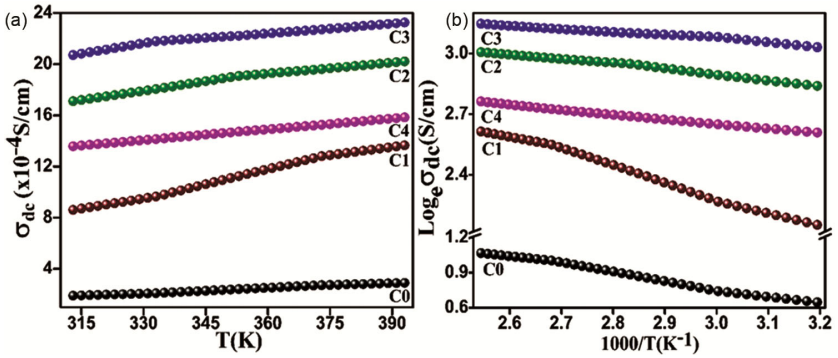

Fig. 6 — DC conductivity (temperature dependent) of PANI and PANI/$Cr(NO_3)_3$ composites.

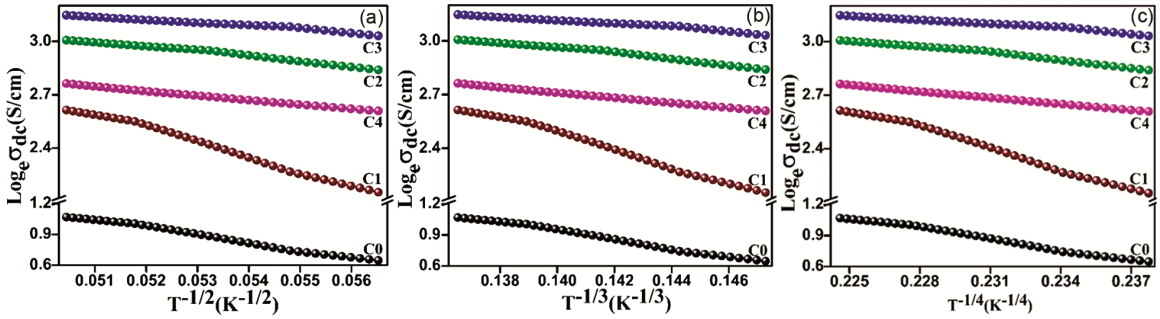

Fig. 7 — (a) Linear Fit of ln σ_{dc} *vs*. $T^{-1/2}$(b) Linear Fit of ln σ_{dc} *vs*. $T^{-1/3}$ and (c) Linear Fit of ln σ_{dc} *vs*. $T^{-1/4}$ for pure PANI and PANI/Cr $(NO_3)_3$ composites.

charge trappings, and an electric dipole persists due to their localized motion. Quasi particles like polarons and bipolarons are formed due to this dipole, and charge transport takes place via these polarons and bipolarons. As the electric field increases, more polarons and bipolarons form, leading to a non-linear increase in the I-V curve[36].

From the I-V characteristics measured for these samples, the dc electrical conductivity (σ_{dc}) values that are estimated at various temperatures at 1V with the help of the equation (6) given below:

$$\sigma_{dc} = \frac{IxL}{VxA} \quad ...(6)$$

here I is the current, A and L are the area and thickness of the sample, respectively, and V is the voltage. The values of σ_{dc} thus calculated are presented in Table 2. The variation of dc conductivity versus temperature for PANI and PANI/$Cr(NO_3)_3$ composites is also shown in Fig. 6.

DC conductivity for PANI and PANI/$Cr(NO_3)_3$ composites varies directly with temperature, possibly because the free charges increase with the rise in temperature[35,36].

DC conductivity (σ_{dc}) data for all the samples were found to follow the Arrhenius relation as mentioned in equation (7) given as

$$\sigma_{dc}(T) = \sigma_0 \exp(\frac{-W}{kT}) \quad ...(7)$$

where W is the electrical conduction activation energy, k is Boltzmann's constant, and σ_0 is the pre-exponential parameter dependent on the nature of the semiconductor.

Using equation (7), the values of activation energy due to electrical conduction can be calculated from the slope of the curve ln (σ_{dc}) versus 1/T. The slope is calculated by linear fitting (as shown in Fig. 6) and presented in Table 2 for all the samples. It is observed from the table the activation energy value due to electrical conduction is found to decrease with an increase in the concentration of chromium nitrate up to 20 weight percent, which implies an increase in conductivity with increasing content of chromium nitrate up to 20 weight percent and after thatits value increases in C4 which means the decrease in conductivity.

In the plot of ln σ_{dc}(T) vs. $T^{(-1/4)}$, it also gives a perfect linear fitting (with linearity ~ 0.999) as represented in Fig. 7 and signifiesthat three-dimensional (3D) transport of charge takes place in all the samples as already explained by equation (8) given as

$$\sigma_{dc} = \sigma_0 e^{-(\frac{T_0}{T})^{\gamma}} \quad ...(8)$$

Table 3 — Mott's three-dimensional VRH parameters were estimated for the samples C0, C1, C2, C3, and C4.

Samples	C0	C1	C2	C3	C4
T_o (K)	0.9871	0.98651	0.9717	0.9568	0.9972
$N(E_F)(cm^{-3}eV^{-1})$	$7.88x10^{27}$	$7.89x10^{27}$	$8.01x10^{27}$	$8.14x10^{27}$	$7.80x10^{27}$
R (cm)	$2.67x10^{-9}$	$2.69x10^{-9}$	$2.68x10^{-9}$	$2.67\ x10^{-9}$	$2.70x10^{-9}$
W (meV)	$1.55x10^{-3}$	$1.55x10^{-3}$	$1.54x10^{-3}$	$1.54x10^{-3}$	$1.55x10^{-3}$
∝R	$89.84x10^{-3}$	$89.82x10^{-3}$	$89.48x10^{-3}$	$89.14x10^{-3}$	$90.07x10^{-3}$
σ_{dc} (S/cm) at RT	$1.91x10^{-4}$	$8.61x10^{-4}$	$17.11x10^{-4}$	$20.72x10^{-4}$	$13.59x10^{-4}$
N_H	$4.07x10^{26}$	$4.08x10^{26}$	$4.14x10^{26}$	$4.20x10^{26}$	$4.03x10^{26}$

where T_0 is the Mott's characteristic temperature related to the degree of localization for the electronic wave function, and σ_0 is the higher temperature limit of conductivity. The exponent $\gamma = 1/(1+d)$ represents the conducting medium dimension.

Mott's VRH model was proposed to explain the VRH of disordered materials in the low-temperature range. But for the present composites, this model is apt to describe the data of dc conductivity even at high temperatures. The values of T_0 and $\ln\sigma_0$ are obtained from the slopes and intercepts of the plots as mentioned earlier and are presented in Table 3.

The mechanism for the conduction of the present composites could be comprehended better in terms of Mott's conduction parameters. Thus, for estimating Mott's VRH parameters, the samples were examined for three-dimensional hopping (*i.e.*, for n=1/4). Mott's characteristics temperature (T_o) is the measurement of the state density plus localization length and finding out the thermal activation hopping between the levels of the off-localized energy in the disarranged materials of different energies. The pre-exponential factor (σ_0) and Mott's characteristic temperature may be calculated from the intersection and slope of $\log\sigma_{dc}$ versus $T^{-1/4}$ curve, in that order, with the help of the relations given below[37-39].

$$\sigma_0 = R^2e^2\nu_oN(E_F) \quad ...(9)$$

$$T_o = \frac{18.1\alpha^3}{k_BN(E_F)} \quad ...(10)$$

where ν_o is the phonon or attempt frequency (~10^{13} Hz) that is evaluated by the Debye temperature, and it depends on the interaction strength of the electron-phonon as well as phonon density of states, $r_p$is polaron radius, $N(E_F)$ is the density of state at Fermi level, R is the average hopping distance within the two energetically closest sites, and $\boldsymbol{\alpha}(=1/r_p)$ is exponential decay coefficient for the localized states in the jumping process. The average hopping distance between the final and initial localized energy states could be determined by the use of the following relation

$$R = \left\{\frac{9}{8\pi\propto k_BTN(E_F)}\right\}^{1/4} \quad ...(11)$$

The average hopping energy of polaron (W) can be defined as the energy required for the hopping of charge carriers from the fully filled energy states to vacant energy states;available for jumping of charge carriers is another essentialfactor for the study of the phenomenon of charge transport, and it could be readily determined by use of the following expression provided the values of R and $N(E_F)$ are known,

$$W = \frac{3}{4\pi R^3N(E_F)} \quad ...(12)$$

The hopping probability would be highest for a strong association in W and R within the constraint that the energy window k_BT must be relatively constricted so that the Fermi energy and localization length remains nearly constant. All of the parameters related to Mott's three-dimensional variable range hopping conduction, determined by the expression (8)-(11) for PANI/chromium nitrate composites, are shown in Table 3.

It has been observed from Table 3 that the average value of hopping distance plus the average hopping energy requisite for jumping from one localized energy state to other energetically favorable localized energy state decreases with the loading concentration of chromium nitrate. This implies the increase in the localized energy states or the localized energy states are very tightly packed, and the jumping of polarons occurs with a lower hopping energy. The lowering of Mott's characteristic temperature with the chromium nitrate loading further substantiates the reduction in the hopping distance and the necessity for lower hopping energy[37,40-42]. Also, it could be noticed from the enhancement in the density of states ($N(E_F)$) at the Fermi energy level. The credibility of Mott's VRH conduction may be examined based on Mott's conditions that $W>>k_BT$ and $\boldsymbol{\alpha}R>1$, and it has been observed that if these two conditions are fulfilled, then Mott's VRH conduction for charge

transport is followed by current PANI/chromium nitrate composites.

4 Conclusions

Pristine PANI and its composites with chromium nitrate were synthesized via in-situ synthesis using the chemical oxidative polymerization method. Comparing XRD, SEM, and FTIR spectra of pristine samples and the composites suggests the dispersion of chromium nitrate particles in the polymerization reaction. The TG analysis and calculated parameters show that thermal stability increases with an increase in the concentration of chromium nitrate up to 20 weight percent in PANI/$Cr(NO_3)_3$ composites and decreases after that. The temperature-dependent dc conductivity of PANI/$Cr(NO_3)_3$ composites has been calculated in the temperature range 313K to 393K using Ohm's law, and it is observed that PANI/chromium nitrate composites show a higher value of dc conductivity in comparison with pure PANI. DC conductivity of PANI and PANI/chromium nitrate composite varies directly with temperature.

The activation energy values for electrical conduction have also been calculated using Arrhenius law. Mott's 3-dimension variable range hopping model is found to applyto PANI and PANI/$Cr(NO_3)_3$ composites, even at high temperatures. The frequency-dependent conductivity of PANI/chromium nitrate composites has been found to follow the same variation with changing concentration as that of dc conductivity obtained by Ohm's law.

References

1 Singh S K, Shukla R K, Kumar R, Tripathi U K & Mishra S K, *Mater Lett*, 309 (2022) 131325.
2 Kalaiarasi J, Balakrishnan D, Al-Keridis L A, Al-mekhlafi F A, Farrag M A, Kanisha C C, Murugan M & Pragathiswaran C, *J King Saud Univ Sci*, 34 (2022) 101824.
3 Lin Y, Li D, Hu J, Xiao G, Wang J, Li W & Fu X, *Phys Chem C*, 116 (2012) 5764.
4 Palliyalil S, Chola R K V, Vigneshwaran S, Poovathumkuzhi N C, Chelaveettil B M & Meenakshi S, *Environ Technol Innov*, 28 (2022) 102586.
5 Mostafaei A & Nasirpouri, *Prog Org Coat*, 77 (2014) 146.
6 Jang J, Ha J & Kim K, *Thin Solid Films*, 516 (2008) 3152.
7 Saini P, Kaushik S, Sharma R, Chakravarty D, Raj R & Sharma J, *Eur Phys J B*, 89 (2016) 137.
8 Saini P, Arora M, Gupta G & Gupta B, Nanoscale, 5 (2013) 4330.
9 Modak P, Kondawar B S &Nandanwar D V, *Mater Sci*, 10 (2015) 588.
10 Shen P K, Huang H T & Tseung A C C, *J Electrochem Soc*, 139 (1992) 7.
11 Janeoo S, Sharma M, Singh G & Goswamy J, *AIP Conf Proc*, 1731 (2016) 050096.
12 Arora R, Mandal U K, Sharma P & Srivastav A, *Mater Today Proc*, 2 (2015) 2215.
13 Rajivgandhi G, Muruthupandy M, Muneeswaran T, Ramachandran G, Manoharan N, Quero F, Anand M & Song J, *Microb Pathog*, 127 (2019) 267.
14 Asha, Goyal S L, Kumar D, Kumar S & Kishore N, *Indian J Pure Appl Phys*, 52 (2014) 341.
15 Goyal S L, Sharma S, Jain D & Kishore N, *Indian J Pure Appl Phys*, 53 (2015) 456.
16 Lee Y J, Lee H S, Lee C G, Park S J, Lee J, Jung S & Shin G, *Appl Sci*, 10 (2020) 6710.
17 GiljaV, Vrban I, Mandic V, Zic M & Murgic Z H, *Polymers*, 10 (2018) 940.
18 Mitra M, Kulsi C, Chatterjee K, Kargupta K, Ganguly S, Banerjee D & Goswami S, *RSC Adv*, 5 (2015) 31039.
19 Mahmoud W E & Al-Ghamdi A, *Polym Adv Technol*, 22 (2011) 877.
20 O'Neil M J, Heckelman P E, Dobbelaar P H & Roman K J, *The Merck Index: R Soc Chem*, 15 (2013).
21 Kashian S, Daneshvar H, Rezaeian P & Rafiean M, *Rad Phys Eng*, 3 (2022) 43.
22 Reddy K R, Sin B C, Ryu K S, Noh J & Lee Y, *Synth Methods*, 159 (2009) 1934.
23 Pouget J P, Hsu C H, MacDiarmid A G & Epstein A J, *Synth Methods*, 69 (1995) 119.
24 Pal R, Goyal S L & Sharma S, *AIP Conf Proc*, 2115 (2019) 030217.
25 Pal R, Goyal S L & Rawal I, *Iran Polym J*, 31 (2022) 110867.
26 Pal R, Goyal S L, Rawal I & Gupta A K, *Solids*, 169 (2022) 110867.
27 Pal R, Goyal S L, Rawal I & Asha, *Mater Sci Eng B*, 270 (2021) 115227.
28 OzkazancE, Zor S, Ozkazanc H, Guney H Y & Abaci U, *Mater Chem Phys*, 133 (2012) 356.
29 Dey A, De S, De A & De S K, *Nanotechnology*, 15 (2004) 1277.
30 MachappaT & Ambika Prasad M V N, Bull Mater Sci, 35 (2012) 75.
31 Ganesan R & Gedanken A, *Nanotechnol*, 19 (2008) 435709.
32 DumitrescuI, Nicolae C A, MocioiuA M, Gabor R A, Grigorescu M & Mihailescu M, *UPB Sci Bull*, 71 (2009) 63.
33 Gupta R, Kumar V, Goyal P K, Kumar S & Goyal S L, *Adv Appl Sci Res*, 3 (2012) 2766.
34 ReghuM, Cao Y, Moses D & HeegerA J, *Phys Rev B*, 47 (1993) 1758.
35 Jain N, Patidar D, Saxena N S & Sharma K, *Indian J Pure Appl Phys*, 44 (2006) 767.
36 Li J, Cui M, Lai Y, Zhang Z, Lu H, Fang J & Liu Y, *Synth Met*, 160 (2010) 1228.
37 Rawal I & Kaur A, *J Appl Phys*, 115 (2014) 043717.
38 Kumar A, Singh R K, Singh H K, Srivastava P & Singh R, *J Appl Phys*, 115 (2014) 103702.
39 Singh R K, Kumar A & Singh R, *J Appl Phys*, 107 (2010) 113711.
40 Nandi D, Ghosh A K, Gupta K, De A, Sen P, Chowdhury A D & Ghosh U C, *Mater Res Bull*, 47 (2012) 2095.
41 Maddison S &Tansley T L, *J Appl Phys*, 72 (1992) 4677.
42 Jan R, Habib A, Akram M A, Ahmad I, Shah A, Sadiq M & Hussain A, *Mater Res Express*, 4 (2017) 1.